E-13713

Comparison of the Oxidation Rates of Some New Copper Alloys

Linus U.J. Thomas Ogbuji and Donald L. Humphrey
QSS, Inc., NASA Glenn Research Center, Cleveland Ohio 44135

Abstract
Copper alloys were studied for oxidation resistance and mechanisms between 550 and 700°C, in reduced-oxygen environments expected in rocket engines, and their oxidation behaviors compared to that of pure copper. They included two dispersion-strengthened alloys (precipitation-strengthened and oxide-dispersion strengthened, respectively) and one solution-strengthened alloy. In all cases the main reaction was oxidation of Cu into Cu_2O and CuO. The dispersion-strengthened alloys were superior to both Cu and the solution-strengthened alloy in oxidation resistance. However, factors retarding oxidation rates seemed to be different for the two dispersion-strengthened alloys.

***Key words**: copper alloys, oxidation, low-oxygen environments, kinetics, mechanisms*

Introduction

Advanced processing techniques are enabling new copper alloys that exhibit superior mechanical properties at elevated temperatures while retaining most of the excellent thermal properties of Cu. One important application for these alloys is in liners for rocket engine combustion chambers. These liners are subject to extreme heat fluxes and severe mechanical stresses. In that application there is a high potential for oxidation and the related problem of blanching from oxidation-reduction cycling induced by fluctuating thermochemical environments [1]. Resistance to oxidation implies resistance to blanching and is hence a major requirement for copper alloys intended for application in reusable launch vehicle (RLV) liners. When a liquid hydrogen/liquid oxygen ("LH2-LOX") rocket engine operates around the stoichiometric oxygen-to-fuel ratio for increased efficiency, the partial pressures of oxidants and reductants are very finely balanced [2]. Minor fluctuations at any location can cause the micro-ambient to flip-flop repeatedly between oxidizing and reducing conditions, leading to blanching. NARloy-Z (Cu-3wt%Ag-0.5wt%Zr), which is used in the current liner of the Space Shuttle main engine (SSME), exhibits pronounced blanching in service [1,2]. The next generation of RLVs calls for significantly longer lives and improved reliability compared to the SSME. To meet these requirements, blanching-resistant alloys and/or coatings are needed.

A new copper alloy, GRCop-84 (Cu - 8a/o Cr - 4a/o Nb) has significantly improved high-temperature mechanical properties, with only a 25% reduction in thermal conductivity relative to Cu [3]. Studies are underway to assess the oxidation and blanching resistance of GRCop-84. Earlier results demonstrated that the oxidation resistance of GRCop-84 in air and in oxygen is superior to those of Cu and NARloy-Z in the 500-700°C temperature range expected of an RLV liner wall [4]. However, a combustion chamber is not under atmospheric pressure. The prevailing partial pressure of oxygen in a rocket chamber is a strong function of the fuel-oxidant stoichiometry [1,2]. Inhomogeneities being inevitable in the mixing and combustion of O_2 and H_2 in practical rocket engines, oxygen partial pressures can vary in the circumferential direction around the chamber wall, and along the axial direction as well. Consequently, the severity of chamber wall oxidation will vary from one point to another, and it is important to assess the oxidation resistance of liner materials under the different $p(O_2)$ values that may prevail in service.

As in prior work [4], NARloy-Z was chosen as the benchmark for GRCop-84 oxidation comparison, but another copper alloy was added to broaden the baseline. "GlidCop", is an oxide-dispersion-strengthened (ODS) alloy comprised of nano-disperse Al_2O_3 particles in copper. The alloys in this study represent compositions of current interest to the aerospace industry, and dispersion strengthening is the best way to improve the mechanical properties of copper for aerospace structural applications without a severe penalty in thermal conductivity. The first GlidCop material included in this study, Glidcop A-L15, contains 0.15wt% Al (or 0.30 wt% Al_2O_3). It exhibited a pronounced oxidation resistance similar to that of GRCop-84, another dispersion-strengthened alloy. Hence, other GlidCop alloys, AL-25 (0. 5 wt% Al_2O_3) and AL-60 (1.1 wt% Al_2O_3), were added in an effort to explore the effect of dispersoid quantity on oxidation resistance.

Experimental Procedure

The GRCop-84 and NARloy-Z materials have been described elsewhere [4]. Briefly, the former was in the form of extruded bars; the latter was in the form of rolled plate. The GlidCop alloys were obtained from the manufacturer, OMG Inc., as either rolled strip (AL-15) or rolled bars (AL-25 and AL-60). All the materials were cut into coupons 19.1

mm (0.75") in diameter and 1.0 mm (0.04") thick, with 3mm (0.12")-diameter hanging holes near the rims, and polished through a 1000 grit finish. They were oxidized for 10-hour durations in a thermogravimetric analyzer (TGA) at temperatures ranging from 550 to 750°C. The oxidant was purified oxygen, buffered by ultra-high-purity (UHP) argon in various proportions. Those proportions were aimed at increasing oxygen content in approximately 10-fold steps, but the exact compositions were dictated by the practicality of mixing the gases from pressurized bottles. The oxygen contents were 2.2, 0.25, and 0.0332 volume % at 1.0 atmosphere overall pressure. The gas mix was flowed into the TGA at 100 cm^3/min.

Results and Discussion

For the purpose of compact labeling, the alloys used in this study are represented in the following figures and charts as GR-84 for GRCop-84, GC-15 for GlidCop AL-15 (and ditto for GC-25 and GC-60), NAR-Z for NARloy-Z, and OF-Cu for OFHC-Cu (oxygen-free, high-conductivity copper).

Weight Gains and Oxidation Rates

Fig. 1 shows histogram plots of the respective specific weight gains after 10 hours under various conditions of reduced oxygen pressures. The trends are more obvious in Fig. 2 where the results are normalized by dividing with the weight gains of Cu under the same conditions. The GlidCop alloys AL-15 and AL-25 registered the least weight gains at all temperatures and oxygen levels; GRCop-84 was next, with comparably low weight gains, especially at the higher temperatures. Above 600°C NARloy-Z showed the least oxidation resistance among the alloys. It gained 75-100% as much weight as did Cu.

Fig. 3 shows results obtained in 100% O_2 for all the alloy, except GlidCop AL-25 and AL-60. At the top is a histogram of weight gains, and at bottom specific weight gains normalized by division with the Cu weight gain. The trends and ranking of the alloys are the same as in reduced oxygen environments. Note, in particular, that NARloy-Z had weight gains that were on par with those of Cu, while GRCop-84 and GlidCop AL-15 showed the strongest resistance to oxidation at all temperatures. It is interesting that

absolute weight gains in 100% O_2 were not significantly higher than the corresponding values in 2.2% or even 0.25% O_2 shown in Fig. 1. This result was confirmed for GRCop-84 in a separate experiment to determine the effect of oxygen partial pressures on the parabolic rate constants, the results of which are shown in Fig. 4. UHP air was used for 20% O_2, and the 0.033% O_2 test was omitted in this experiment because oxidation kinetics were found to be linear rather than parabolic in 0.033% O_2, as shown below.

Oxidation Mechanisms

One aim of this work was to elucidate the mechanism responsible for the relatively superior oxidation resistance of the dispersion-strengthened alloys, GRCop-84 and GlidCop. While the Cr_2Nb precipitates in GRCop-84 do participate in the oxidation process (as has been shown elsewhere [4]), the Al_2O_3 particles in GlidCop cannot play a direct role in retarding oxidation, for two reasons: (1) Unlike Cr_2Nb which undergoes oxidation, Al_2O_3 does not compete with Cu for the consumption of oxygen; and (2) the quantities of Al_2O_3 in GlidCop are too minute, and the temperatures too low, for their coalescence into a continuous and protective Al_2O_3 film. That leaves one mechanism by which the Al_2O_3 particulates in GlidCop might protect it from oxidation: hindrance of diffusion in the classic concept of logarithmic oxidation [5]. Hence, all data acquired in this study was analyzed for linear, parabolic, and logarithmic kinetics, in that sequence.

This was done in a systematic manner because accurate discrimination between oxidation mechanisms is seldom easy [6,7]. The recognition of logarithmic kinetics is especially difficult. Generally, it is conceptualized as *sub-parabolic* (i.e. slower-than-parabolic) rate of oxidation [5, 6]. However, "logarithmic" has also been employed to describe a hybrid process in which linear and parabolic mechanisms are both active during oxidation [7]. In analyzing the data, parabolic and logarithmic oxidation were investigated only when the linear plot (specific weight gain $\Delta w'$ against time) exhibited a convexity indicating slower-than-linear kinetics. In that case parabolic behavior was assumed if the plot of $\Delta w'$ versus square root of time was linear with a regression R^2 value exceeding ~0.95. When that test also failed, a plot of $\Delta w'$ against the log of time was made to confirm logarithmic kinetics. Strictly speaking, logarithmic behavior is described by the equation:

$$\Delta w'(t) = k_1 \log(k_2 t + k_3),$$

where $\Delta w'(t)$ is specific weight gain after time t, and the k_i are characteristic constants. These constants are not usually known a-priori but k_3 is generally assumed to be ~1[5, 8]. Therefore, if k_3 is ignored, a linear dependence of $\exp(\Delta w'/k_1)$ on t indicates that kinetics are reasonably logarithmic. But since k_1 is often unknown, the less rigorous plot, $\Delta w'$ versus log (t), is usually employed for the logarithmic test. That was done in this analysis.

The sequenced discrimination for oxidation kinetics is illustrated in Fig. 5 for Cu oxidation in 2.2% O_2. The plot of specific weight gain versus time (top chart) exhibits a concavity indicative of slower-than-linear oxidation kinetics, while the logarithmic plot (bottom chart) displays a convexity indicative of faster-than-logarithmic kinetics. On the other hand, the plot of specific weight gain versus square root of time is linear for all temperatures, confirming that parabolic law prevailed for the oxidation of Cu in 2.2% O_2 at all temperatures studied. Fig. 6 shows that oxide growth law in 2.2% O_2 was parabolic for all the alloys. The data regression results are shown in Table 1. Not only was the R^2 value significantly higher in each case for the parabolic model, but visual inspection of the plots confirmed the superiority of the parabolic model – as illustrated in Fig. 4 for Cu.

Note that the parabolic rate constants (k_p) for GRCop-84 and NARloy-Z were similar at 550 °C but the difference between them grew with increasing temperature until, at 700 °C, k_p was 2.5 mg^2/cm^4hr for NARloy-Z and only one-quarter as much or 0.66 mg^2/cm^4hr for GRCop-84. That is still significantly lower than the order-of-magnitude difference in rates observed between the two materials in 50-hour oxidation exposures [4,9]. This is understandable because 10 hours is not long enough for GRCop-84 to have entered terminal-stage oxidation observed in 50-hour oxidation tests [4]. That final stage of dense oxide scale which retards diffusion kinetics is thought to be responsible for the order-of-magnitude superiority of GRCop-84 in terms of resistance to oxidation. Note also, from Fig. 6, that differences between GRCop-84 and GlidCop AL-15 oxidation rates decreased with increasing temperature -- a trend that is contrary to that between GRCop-84 and NARloy-Z. Therefore, for use at the higher temperatures explored here, GRCop-84 is as good as GlidCop, and both are significantly superior to NARloy-Z.

Oxidation kinetics for the alloys in 0.25% O_2 were very similar to the results obtained in 2.2% O_2 both in the trends and relative oxidation rates. Logarithmic and linear fits were again ruled out for the three alloys by inspection of the plots and by linear regression of the data. The parabolic plots determined by analysis are shown in Fig. 7, and 700°C highest temperature NARloy-Z exhibited about six times the oxidation rates of GRCop-84 and Glidcop-AL15. At 550°C the parabolic rate constants of GRCop-84 and NARloy-Z were comparable. This is understandable: At low temperatures there is little oxidation of the Cr_2Nb precipitates in GRCop-84, making it behave more or less like NARloy-Z. A comparison of Tables 1(b) and 2(a) shows that oxidation rate constants in 0.25% O_2 were similar to those in 2.2% O_2. As shown in Fig. 4, this fact was confirmed for GRCop-84 with repeat experiments. It reflects a fundamental similarity of the underlying oxidation mechanisms for these alloys. The exclusive or by far dominant oxidation process for each of these materials is oxidation of the Cu matrix, and its rate is controlled by the diffusion of Cu species outwards through the oxide to the gas interface where it reacts with the O species. It is reasonable that the diffusion rate of Cu through its oxides is not sensitive to the partial pressure of oxygen at the surface. Oxidation in 0.033% O_2 was an exception to this observation (below).

Fig. 8 shows oxidation data for Cu and the alloys in 0.033% O_2. Apart from the slightly irregular curves for GRCop-84 at the two lower temperatures, the trends of weight gain between the alloys were similar to those seen in 2.2 and 0.25% O_2. A major difference is that the kinetics in 0.033% O_2 were essentially linear for all four materials at 550°C and strictly linear from 600°C to 750°C. Though the plots for all four materials appear to exhibit a slight deviation from linearity at 550°C, the respective plots of the same data for parabolic and logarithmic models showed even stronger curvatures. Therefore, linear oxidation is assumed to prevail in 0.033% O2, and the linear rate constants are given in Table 2(b) along with the regression factors. Specific weight gains averaged a third to half as much in 0.033% as in 0.25% O_2 for each material. Thus, weight gains in 0.033% O_2 were sharply different from those at higher oxygen levels -- where weight gains and rates did not scale up with $p(O_2)$. It appears that at 0.033%O_2 oxygen concentrations at

the gas interface are so low that overall rate is limited by reaction rather than by Cu diffusion, hence the linear kinetics.

The consistency between these materials in all cases is noteworthy, but not surprising. When kinetics are linear (in 0.033% O_2), they are linear for all four materials; and when they are parabolic (0.25% - 100% O_2), they are so for all of them. That probably reflects the fact that in all cases the main reaction is the oxidation of copper to its usual, duplex Cu_2O/CuO scale [4, 8, 9]. The difference in detail may reflect the roles of the dispersed particulates. For instance, in the case of GRCop-84 it was suggested that its significantly lower oxidation rate than Cu and NARloy-Z reflects the consumption of extra O_2 by the oxidation of Cr_2Nb precipitates [4]. Also, it is possible that the fine particulates, where they are present, affect kinetics by hindering cation out-diffusion in the main reaction (the oxidation of Cu) and/or anion inward diffusion in the subsidiary reaction (oxidation of the Cr_2Nb particles).

It was hoped that the GlidCop alloys would reveal a mechanism of oxidation retardation involving the hindrance of diffusing species. If the dispersoids were inhibiting diffusion, that effect should scale with Al_2O_3 content. That was not the case. Fig. 9 compares specific weight gains by the three GlidCops alloys in the three environments between 550°C and 700°C. In nearly all cases AL-60, the Glidcop variety with the highest Al_2O_3 content, gained more weight than AL-25 and AL-15. Also, AL-15 and AL-25 seem to leap-frog each-other in a random manner. It is not clear why Glidcop AL-60 lacks the pronounced oxidation resistance of AL-25 and AL-15, or why the other two compositions have such good oxidation resistance in the first place.

The superior oxidation resistance of GRCop-84 in this temperature regime has been attributed to the consumption of extra oxygen to oxidize Cr and Nb in the precipitates [4]. However, no equivalent mechanism exists for Glidcop. Logically, oxidation suppression in GlidCop must somehow relate to the dispersed Al_2O_3 particles. The microstructures are all similar in that there is a random distribution of the Al_2O_3 particles, some of which are indicated with arrows in the TEM image (Fig. 10c). The Cu grain outlines are evident

in each case, and the Al_2O_3 particle distribution does not appear to favor the Cu grain boundaries. Preferential distribution of precipitates at Cu grain boundaries would suggest a mechanism to account for the slower oxidation rates of GlidCop (and GRCop-84). Grain boundaries are the primary diffusion path for Cu oxidation in this temperature regime [9], and the phenomenology of logarithmic kinetics is thought to be blockage of such short-circuit diffusion pathways [5]. However, these microstructures show no Al_2O_3 preference for Cu grain boundaries, and this agrees with the plots above, which show no sign of logarithmic oxidation kinetics in GlidCop.

Fig. 11 shows the GRCop-84 microstructure. Again the outlines of Cu grains are obvious. There are precipitates at some grain boundaries (inset), as should be expected, given the 14 vol% precipitate loading in this alloy. However, the overall precipitate distribution is clearly random. A more thorough examination of GRCop-84 by TEM tilt experiments was reported to reveal a weak correlation between Cu grain boundaries and the primary Cr_2Nb particles, which grow from the melt during casting of GRCop-84. However, such a correlation must be weak, as Fig. 11 indicates no pronounced preference of precipitates for grain boundaries. This conclusion is supported, as in the case of GlidCop, by the absence of logarithmic kinetics in the plots of oxidation rates. A probable explanation for the oxidation resistance of GRCop-84 under the conditions of this study remains the same as in ref. 4. The kinetics are slowed by diffusion of extra oxygen through the Cu_2O/CuO oxide scale to oxidize the Cr_2Nb.

Of course, this explanation does not apply to the comparably slow oxidation of GlidCop alloys, and whatever the oxidation resisting mechanism in GlidCop, it does not seem to scale with the concentration of dispersed Al_2O_3.

Analysis of Oxide Scales

Table 3 shows the constituents of oxide films on some of the alloys, after exposure in 2.2% oxygen, at 600 and 700°C. (The constituents of oxides grown in 0.033% O_2 were almost identical.) The analyses were obtained by x-ray diffractometry from the sample surfaces after the oxide films had completely spalled off, and from the oxide film after it

was pulverized. In NARloy-Z the appearance of ZrO_2 (albeit in trace amounts) only at the oxide/substrate interface shows that, as in the case of GRCop-84 [4], secondary oxidation (of Zr) occurred by reaction with oxygen diffusing in across the oxide film. However, the amount of Zr in this alloys (0.1%) was too small for this secondary oxidation to influence overall kinetics.

In GlidCop (AL-15 and AL-60) Al_2O_3 was not detected in, on, or under the oxide film after oxidation in any environment, at any temperature studied. The amount of Al_2O_3 in the GlidCop alloys was below the XRD detection threshold. Still, if oxidation retardation involved "protection" by Al_2O_3 in the usual sense, one might expect to see all the Al_2O_3 displaced in the new oxide to have collected as a continuous film at the substrate/oxide or oxide/gas interface. This did not happen because the temperatures were too low for the diffusion of constituents that would be necessary to reassemble the Al_2O_3 as a protective film. Hence, the superior oxidation resistance of the GlidCop alloys does not seem to lie in a protective layer of Al_2O_3, and it remains unexplained for now.

Summary and Conclusions

Oxidation rates of Cu and three of its important alloys have been studied in reduced-oxygen environments between 550 and 750°C. In 332 ppm O_2 all the materials oxidized with linear kinetics, while at higher O_2 levels they all oxidized with parabolic kinetics. In general, Cu and NARloy-Z showed the least resistance to oxidation, while GRCop-84 and the GlidCop alloys showed the highest oxidation resistance. The microstructures show that precipitates (Cr_2Nb in GRCop-84 and Al_2O_3 in GlidCop) are essentially randomly distributed in the respective Cu matrices, leaving no grounds to suspect logarithmic oxidation in these two oxidation-resistant alloys. This agrees with the kinetic plots, which show no logarithmic components. For oxidation resistance in oxygen-lean environments around 700°C, GRCop-84 and GlidCop perform the best. Dispersion strengthened alloys (GRCop-84 and GlidCop) are superior to solid-solution-strengthened alloys (NARloy-Z) and the base alloy (Cu) in terms of oxidation resistance. In the alloys, as in copper, the primary oxidation reaction is oxidation of Cu to Cu_2O and CuO. It is unclear how the dispersoids affect this reaction, but in GRCop-84 overall kinetics are

slowed by the additional oxidation of the Cr_2Nb precipitates. It is not clear why GlidCop has such a good resistance to oxidation, and its oxidation rate does not depend on the concentration of Al_2O_3 dispersoids.

Acknowledgments

This work was performed at NASA Glenn Research Center under the High Operating Temperature Propulsion Components (HOT-PC) and Second-Generation Reusable Launch Vehicle programs of Space Transportation. The authors are grateful to D. Ellis of Case Western Reserve University for the samples, and for a detailed discussion of this work; to T. McCue of QSS, Inc., for the FESEM analysis; and to D. Hull of NASA Glenn Research Center for the TEM imaging.

References

1. D.B. Morgan et al., "Investigation of Copper Alloy Combustion Chamber Degradation by Blanching", Advanced Earth-to-Orbit Propulsion Technology 1988, vol. II, .J. Richmond and S. Wu eds., NASA Conf. Publication 3012 (1988)
2. M. Murphy, et al., "Effects of Oxygen/Hydrogen Combustion Chamber Environment on Copper Alloys", Advanced Earth-to-Orbit Propulsion Technology 1986, vol. II, R.J. Richmond and S. Wu eds., NASA Conf. Publication 2437 (1986) 580
3. D.L. Ellis and D.J. Keller, "Thermophysical Properties of GRCop-84", NASA Contract Report CR 2000-210055, NASA GRC, Cleveland, OH, June 2000
4. L.U.J.T. Ogbuji, "The General Isothermal Oxidation Behavior of Cu-8Cr-4Nb" (submitted to *Materials at High Temperatures.*)
5. D.E. Davies and U.R. Evans, "The Oxidation of Iron at 175 to 350°C", Proc. Roy. Soc. Lond., **225A** (1954) 443-62
6. L.U.J.T. Ogbuji, J. Electrochem. Soc., vol. 145, No. 8 (1998) 2876
7. K. G. Nickel, *Corrosion of Advanced Ceramics*: Measurement and Modelling, K.G. Nickel ed., Kluwer Publishers, Boston USA (1994) 59
8. A. Ronnquist and H. Fischmeister, J. Inst. of Metals, vol 89 (1960-61) 65-76
9. J. –H. Park and K. Natesan, Oxidation of Metals, vol 39 #s5/6 (1993) 411-35
10. J.R. Groza, Materials Characterization 31 (1993) 133

Figure Captions

Fig 1 Histograms showing specific weight gains of Cu and its alloys at different temperatures and reduced oxygen concentrations

Fig 2 Specific weight gains of the alloys normalized to Cu weight gains and plotted against temperature

Fig 3 Specific weight gains of Cu and its alloys in 100% oxygen (1.0 atm.)

Fig 4 Parabolic rate constants for GRCop-84 as a function of oxygen concentration at 650°C; the experiments were repeated three times

Fig 5 Kinetic plots for oxidation of copper in 2.2% O_2, assuming different weight-gain laws

Fig 6 Parabolic plots for the oxidation of three copper alloys in 2.2% O_2 (The corresponding regression factors are shown in Table 1b.)

Fig. 7 Parabolic plots for the oxidation of the copper alloys in 0.25% O_2 (The corresponding regression factors are shown in Table 2a.)

Fig 8 Specific weight gain versus time indicating linear oxidation kinetics for copper and the three alloys in 0.033% O_2

Fig 9 A comparison of specific weight gains for the three GlidCop alloys under the various conditions studied

Fig 10 Micrographs of the GliCop alloys: (a) SEM of AL-60, (b) SEM of AL-25, and (c) TEM of AL-15, indicating random distribution of Al_2O_3 in Cu. (In (b) the inset is magnified 10X relative to the background.)

Fig 11 SEM micrograph of GRCop-84 showing random distribution of Cr_2Nb precipitates in Cu (Inset shows some precipitates at grain boundaries.)

Table 1, Data Regression Results for the 10-h TGA Oxidation of Cu and its Alloys in 2.2% Oxygen

(a) Linear Oxidation Mechanism

Material	Parameter of Fit (R^2 Values)			
	550°C	600°C	650°C	700°C
GRCop-84	0.961	0.944	0.990	0.969
NARloy-Z	0.979	0.961	0.984	0.975
GlidCop AL-15	0.931	0.918	0.929	0.993
OFHC-Cu	0.975	0.972	0.973	0.979

(b) Parabolic Oxidation Mechanism

Material	Parameter (R^2) of Fit and **[k_p in mg^2/cm^4h]**			
	550°C	600°C	650°C	700°C
GRCop-84	0.999 **[0.14]**	0.988 **[0.26]**	0.998**[0.38]**	0.997 **[1.15]**
NARloy-Z	0.999 **[0.12]**	0.999 **[0.36]**	0.995 **1.17]**	0.999 **[2.51]**
GlidCop AL-15	0.981 **[0.05]**	0.974 **[0.11]**	0.997**[0.31]**	0.997 **[0.50]**
OFHC-Cu	0.999 **[0.89]**	0.999 **[1.77]**	0.999 **2.61]**	1.000 **[5.88]**

(c) Logarithmic Oxidation Mechanism

Material	Parameter of Fit (R^2 Values)			
	550°C	600°C	650°C	700°C
GRCop-84	0.984	0.997	0.968	0.987
NARloy-Z	0.980	0.994	0.977	0.986
GlidCop AL-15	0.966	0.969	0.962	0.962
OFHC-Cu	0.985	0.987	0.987	0.981

Table 2(a), Parabolic Regression Results for the 10-h TGA Oxidation of Cu and its Alloys in 0.25% Oxygen

Material	Parameter (R^2) of Fit and **[k_p in mg^2/cm^4h]**			
	550°C	600°C	650°C	700°C
GRCop-84	0.997 **[0.17]**	0.994 **[0.21]**	0.985 **[0.41]**	0.990 **[0.51]**
NARloy-Z	0.982 **[0.12]**	0.997 **[0.31]**	0.999 **[1.15]**	0.998 **[3.21]**
GlidCop AL-15	0.941 **[0.01]**	0.962 **[0.03]**	0.991 **[0.14]**	0.991 **[0.51]**
OFHC-Cu	0.997 **[0.55]**	0.997 **[1.25]**	0.993 **[2.11]**	0.996 **[6.33]**

Table 2(b), Linear Regression Results for the 10-h TGA Oxidation of Cu and its Alloys in 0.033% Oxygen

Material	Parameter (R^2) of Fit and **{k_l in mg/cm^2h}**			
	550°C	600°C	650°C	700°C
GRCop-84	0.945**{0.04}**	0.994**{0.06}**	0.989**{0.11}**	0.997 **{0.12}**
NARloy-Z	0.990 **{0.05}**	0.994**{0.10}**	0.997**{0.14}**	0.999 **{0.19}**
GlidCop AL-15	0.974 **{0.02}**	0.983**{0.03}**	0.970**{0.05}**	0.985 **{0.07}**
OFHC-Cu	0.995 **{0.11}**	1.000**{0.12}**	0.998**{0.15}**	0.999 **{0.20}**

Table 3, Oxidation Products of Cu and Alloys in 2.2% Oxygen

Material	Oxides Found on Samples Oxidized in 2.2% O_2			
	600°C		700°C	
	On Substrate Surface	In Pulverized Oxide Scale	On Substrate Surface	In Pulverized Oxide Scale
NARloy-Z	Cu_2O (Cu, Ag)[1]	Cu_2O, CuO	Cu_2O, ZrO_2[2,3] (Cu, Ag)	Cu_2O, CuO[4]
GlidCop AL-15	Cu_2O (Cu) (@)	Cu_2O, CuO (@)	Cu_2O (Cu) (@)	Cu_2O, CuO (@)
GlidCop AL-60	Cu_2O (Cu) (@)	Cu_2O, CuO (@)	Cu_2O, CuO[4] (@)	Cu_2O, CuO[3] (@)
Cu-Zr	Cu_2O (Cu)	Cu_2O, CuO[4]	Cu_2O (Cu)	Cu_2O, CuO ZrO_2[2,3]

[1] Metallic species detected are in parentheses,
[2] Monoclinic
[3] Trace
[4] Minor
[@] Note: Al_2O_3 not detected

Fig. 1, Weight-Gain Histograms of Cu Alloys

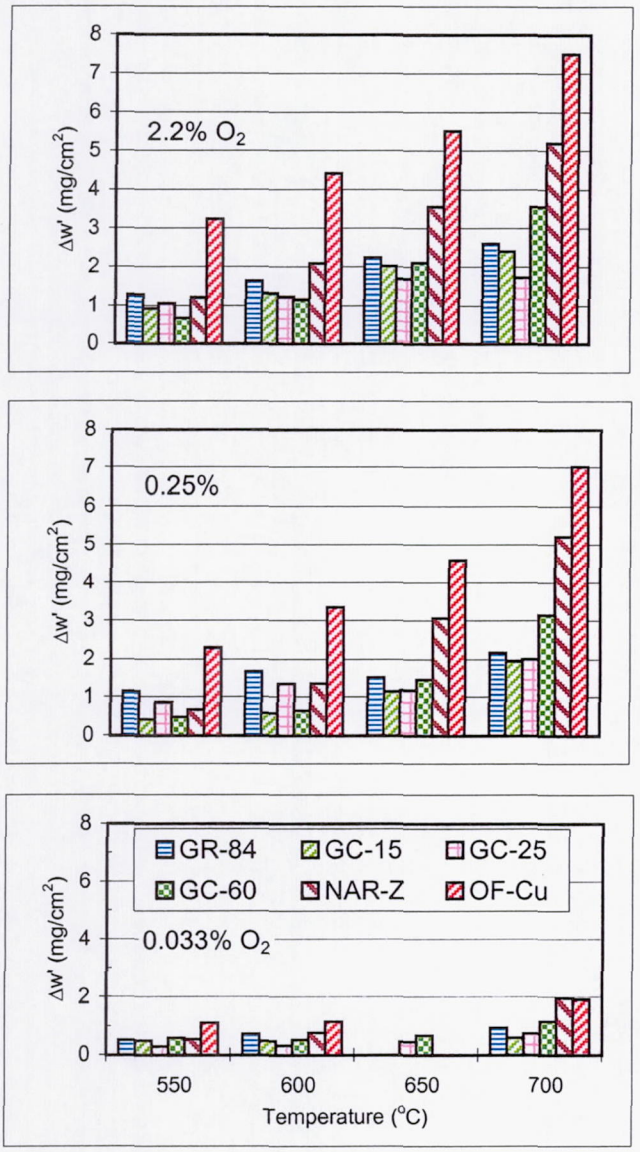

Fig. 2, Normalized Weight Gains of Cu Alloys

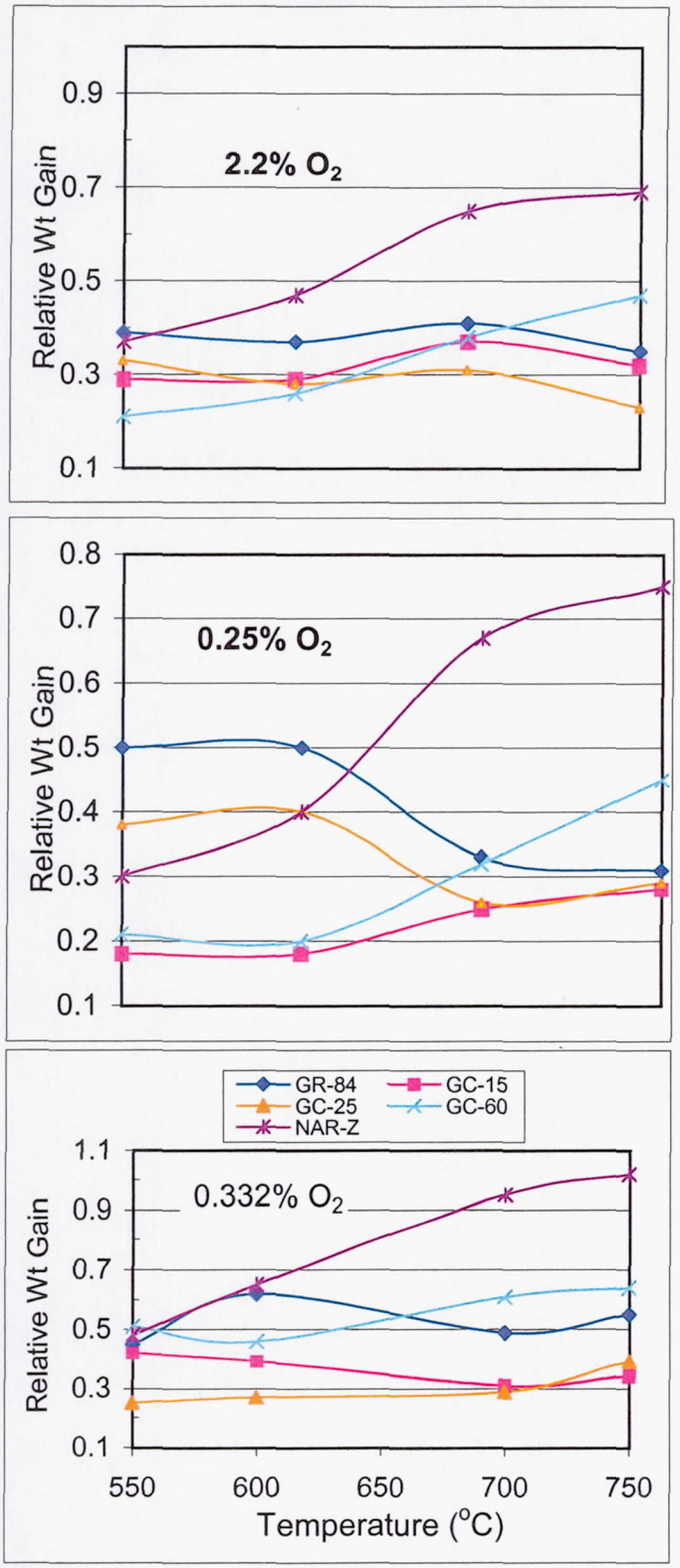

Fig. 3, Weight Gains of Cu & Alloys in 100% O_2

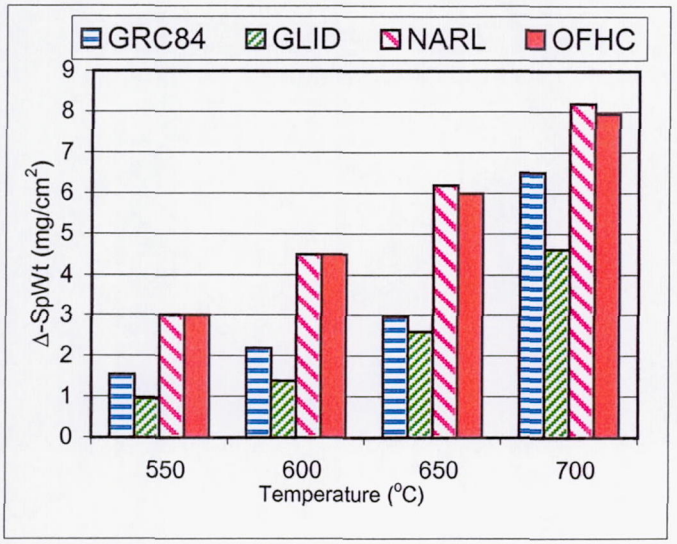

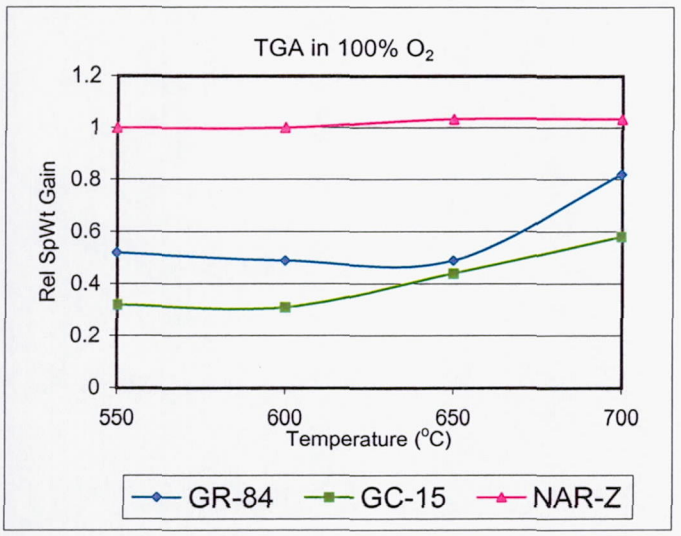

Fig. 4, Parabolic Rate Constants versus Oxygen Concentration

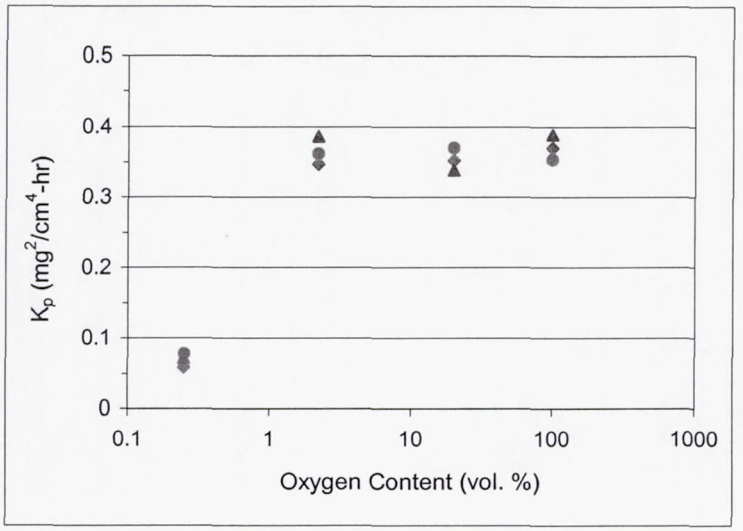

Fig. 5, Comparing Kinetic Plots for Oxidation in 2.2% Oxygen

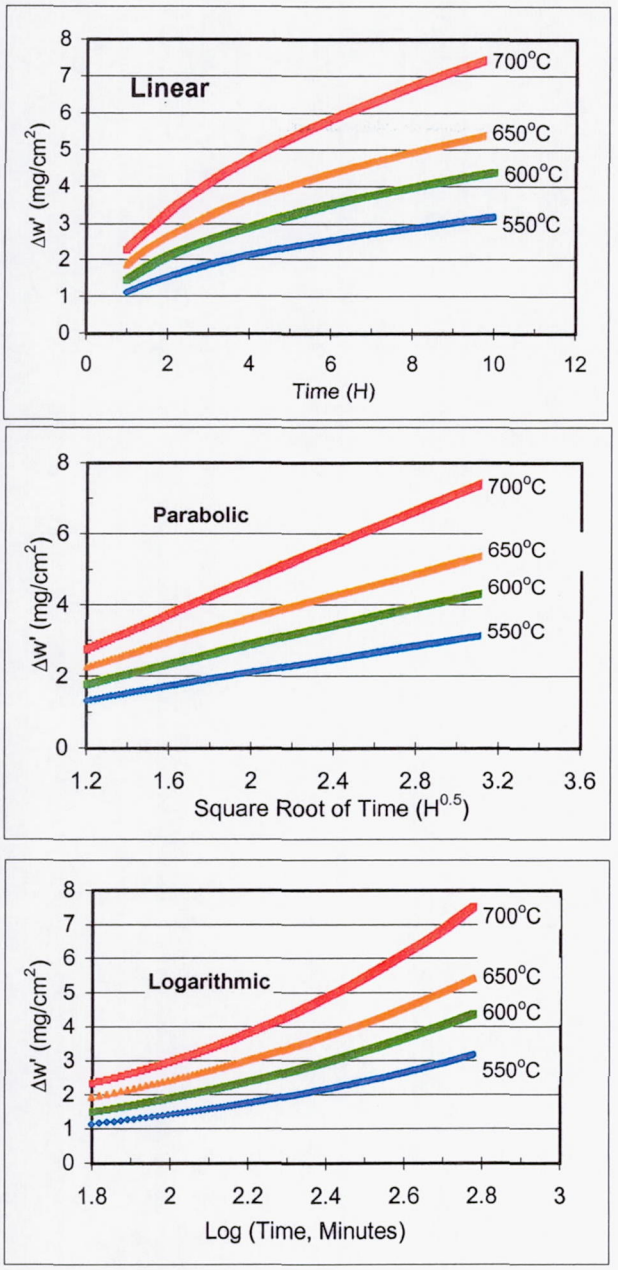

Fig. 6, Parabolic Plots of Oxidation Data in 2.2% Oxygen

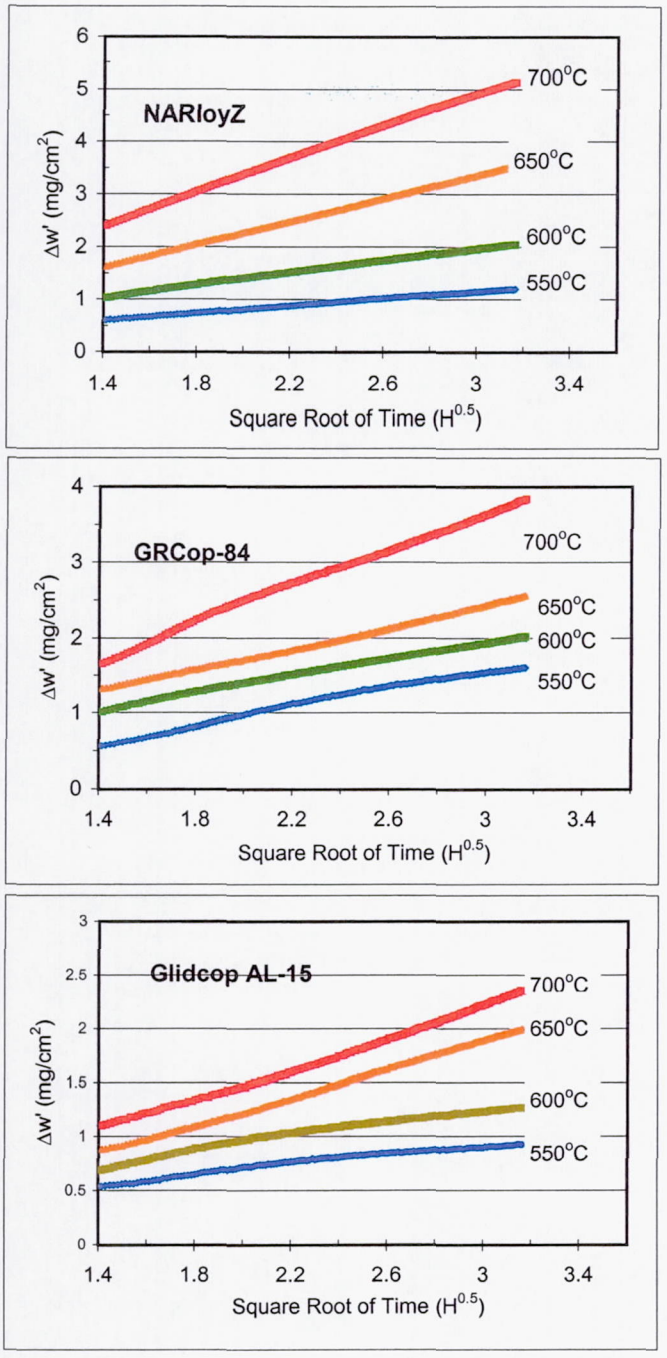

Fig. 7, Parabolic Plots for Alloy Oxidation in 0.25% Oxygen

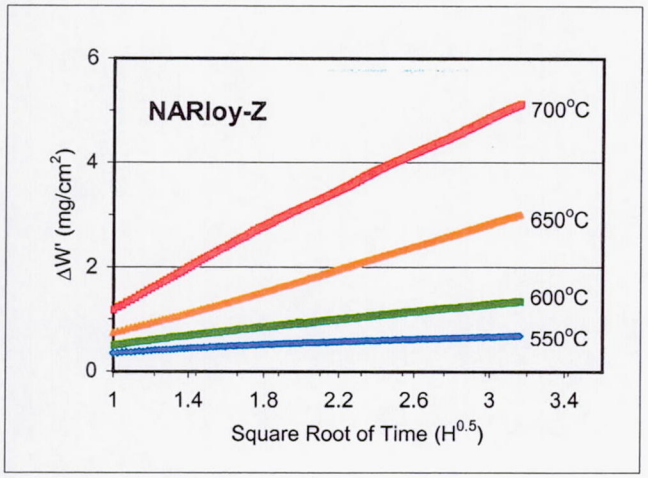

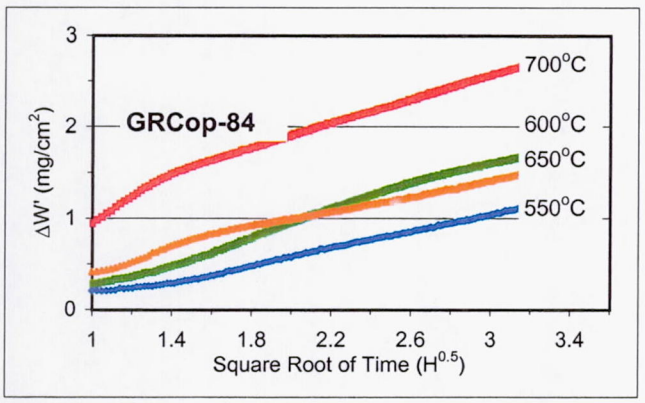

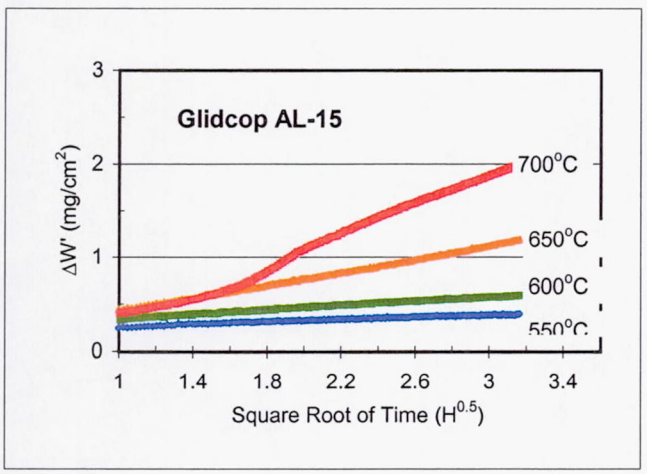

Fig. 8, Linear Kinetics for Oxidation of Cu & Alloys in 0.033% O_2

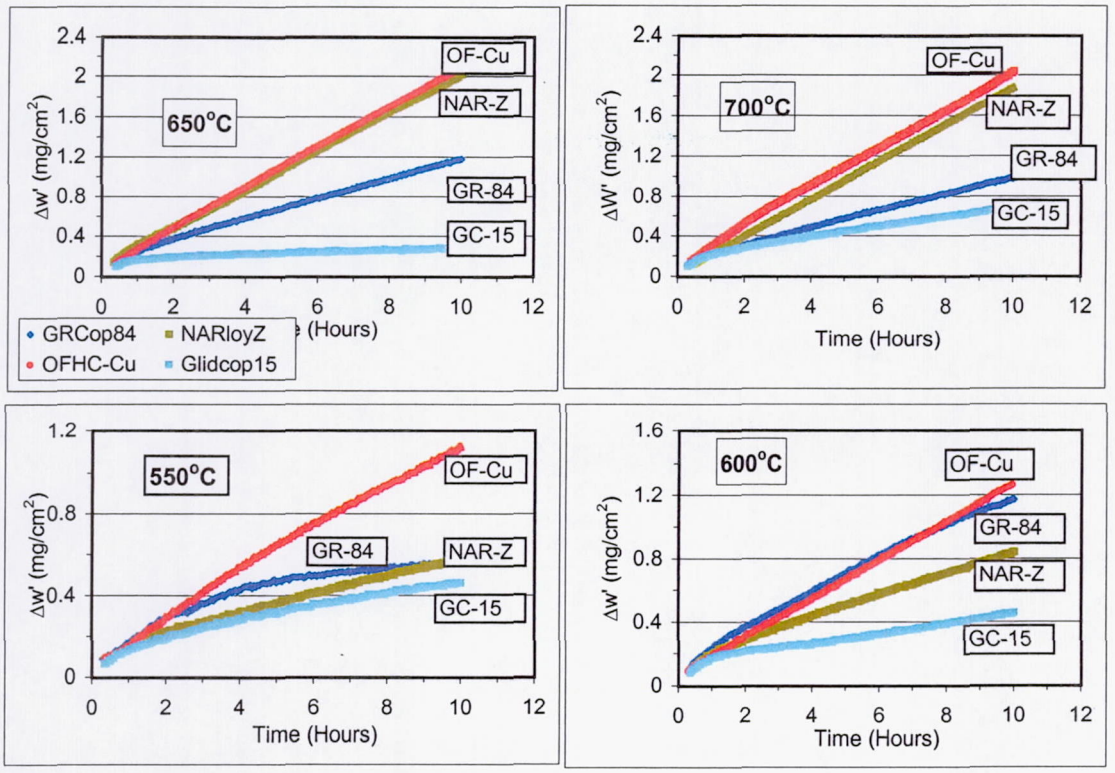

Fig. 9, Comparing Weight Gains of GlidCop Alloys

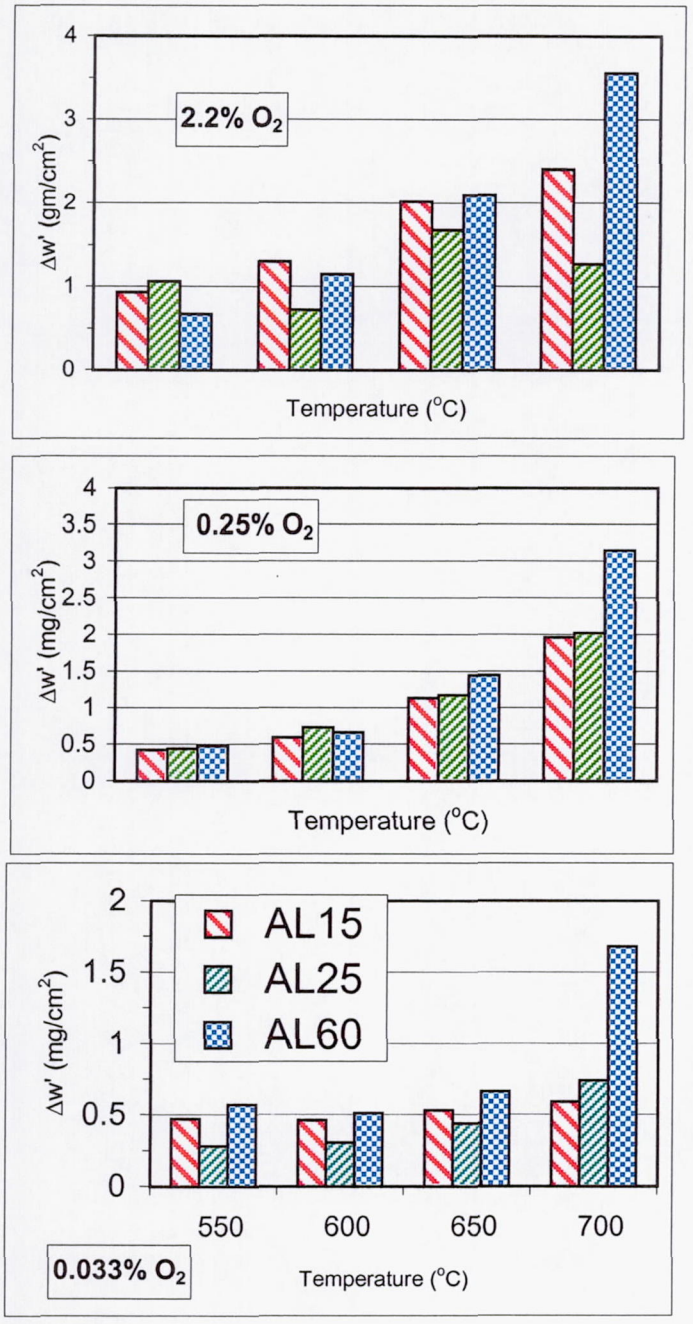

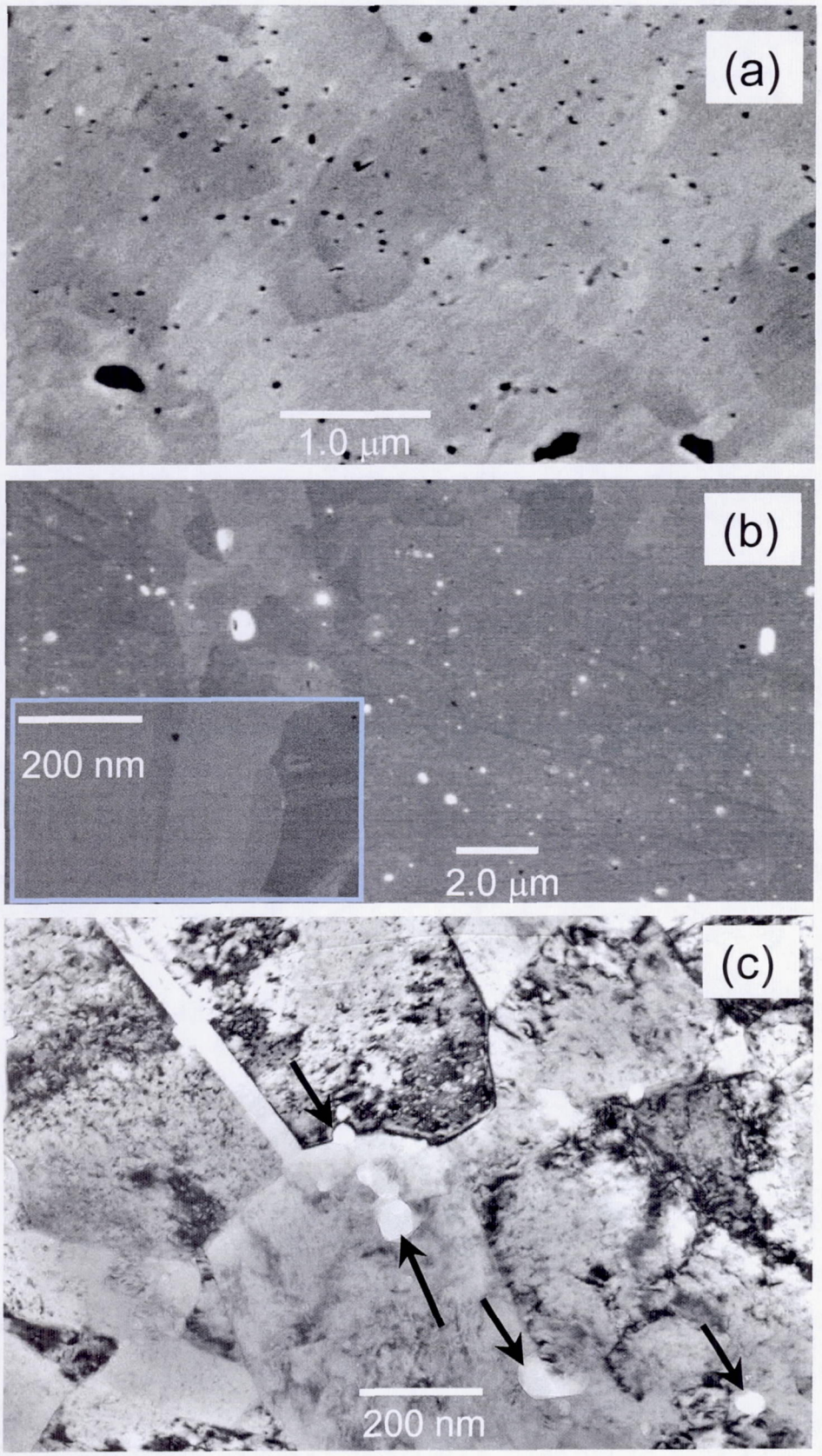

Fig. 10, GlidCop microstructures: (a)AL-15, (b) AL-25, (c) AL-15

Fig. 11, SEM Microstructure of GRCop-84